CHARACTERIZATION OF FLOODED AREAS DUE TO THE 2011 TOHOKU, JAPAN EARTHQUAKE FROM SAR INTENSITY IMAGES

Wen Liu[*1] and Fumio Yamazaki[2]

[1] Graduate student, Department of Urban Environment Systems, Chiba University,
1-33, Yayoi-cho, Inage-ku, Chiba 263-8522, JAPAN; Tel:+81-43-290-3528;
Research Fellow of the Japan Society for the Promotion of Science;
Email: wen_liu@graduate.chiba-u.jp

[2] Professor, Department of Urban Environment Systems, Chiba University
1-33, Yayoi-cho, Inage-ku, Chiba 263-8522, JAPAN; Tel:+81-43-290-3557;
E-mail: fumio.yamazaki@faculty.chiba-u.jp

KEY WORDS: Tsunami, TerraSAR-X, ALOS/PALSAR, SAR intensity image, ASTER DEM, the 2011 Tohoku Earthquake

ABSTRACT: The M_w 9.0 Tohoku earthquake on March 11, 2011, which occurred off the Pacific coast of the northeastern (Tohoku) Japan, caused gigantic tsunamis and brought vast devastation and a huge number of casualties. Various high-resolution satellites quickly captured the details of affected areas, and were used for emergency response. In this study, extraction of flooded areas was carried out using pre- and post-event synthetic aperture radar (SAR) images, which can observe the ground surface regardless of weather and sunlight conditions. Since the water surface generally shows very low backscattering intensity, the flooded areas could be extracted by the difference of SAR intensity between the pre- and post-event images from TerraSAR-X (X-band) and ALOS/PALSAR (L-band). Then, the characterizations of flooded areas were investigated, comparing the results from the X-band and L-band images. A pre-event ASTER DEM with 15m resolution was also employed to detect affected areas by tsunami. Finally, the results were compared with ground truth data to examine the accuracy of the proposed method.

1. INTRODUCTION

The Tohoku earthquake on 11 March 2011 was the most powerful one to hit Japan since modern record-keeping began in 1900. The epicenter was located at 38.322º N, 142.369º E at a depth of about 32 km. The earthquake triggered extremely high tsunamis of up to 40.5 m run-up in Miyako, Iwate Prefecture, caused huge loss of lives and destruction of infrastructures. According to the research by Geospatial Information Authority of Japan (GSI), about 561 km^2 areas were totally flooded by the tsunamis after the earthquake. It is recognized that remote sensing is an efficient tool to monitor the disaster in a wide range by optical and radar sensors. Optical images can grasp detail information easily, but it is limited by weather condition. On the other hand, synthetic aperture radar (SAR) sensor is independent from weather and daylight, and more suitable to map damaged areas reliably and timely.

In the past, there had been several different detection approaches for the derivation of flooding areas. From single SAR image, active contour models (Horritt et al., 1999) have gained popularity as a means of finding smooth water boundaries using tone and texture information. These algorithms had been used for flood boundary delineation by Ahtonen et al. (2002) and Matgen et al. (2007). From multi-temporal images, Heremans et al. (2003) detected flooded areas from ENVISAT/ASAR images by an amplitude based method. Geudtner et al. (1996) and Dellepiane et al. (2000) monitored flooding from C-band SAR interferometry by coherence based techniques. However, interferometry is not very suitable for X-band SAR due to the low temporal correlation.

In this study, two pairs of pre- and post-event SAR intensity images were used to extract the flooded areas due to the Tohoku earthquake tsunami by simply taking the difference of backscatter intensities. The parameters to extract flooded areas were discussed by comparing with optical images visually. Then the results from the X- and L-band SAR were compared to investigate their characteristics, and verified by GIS data of the visually detected inundated areas. Finally, the relationship between the flooded area and digital elevation model (DEM) was described.

2. DATA USED AND IMAGE PREPROCESSING

This study focuses on the coastal zone of Tohoku, Japan, which is the most severely affected area in the 2011 Tohoku earthquake, shown in Figure 1(a). Two TerraSAR-X images taken before and after the earthquake, shown in Figure 1 (b-c), were used to detect flooded areas. The pre-event image was taken on October 20, 2010 (UTC) with 37.3° incidence angle, and the post-event was taken on March 12, 2011 (two days after the earthquake) with the same incidence angle at the center of the image. Both images were taken by HH polarization, in the descending path. Since

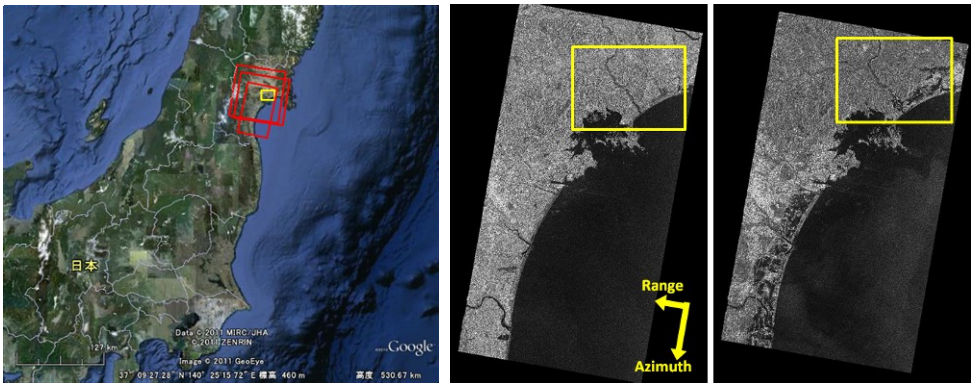

(a) (b) (c)

Figure 1 The SAR data area along the Pacific coast of Tohoku, Japan (a); the pre-event TerraSAR-X image taken on Oct. 21, 2010 (b) and the post-event image taken on March 13, 2011 (c); the target area is shown in the yellow frame.

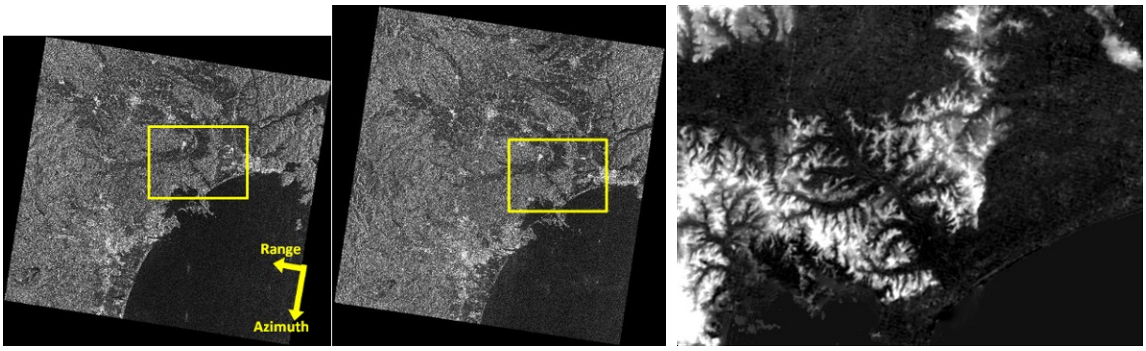

(a) (b) (c)

Figure 2 The pre-event PALSAR image taken on Sep. 11, 2010 (a) and the post-event image taken on March 16, 2011 (b); The pre-event DEM of the target area (c).

they were acquired by StripMap Mode, the azimuth resolution was about 3.3 m and the ground range resolution was about 1.2 m. After the enhanced ellipsoid correction (EEC), two images were geocoded and transformed into those with a pixel size of 1.25 m.

To compare the difference between X-band and L-band, two ALOS/PALSAR images were also employed, as shown in Figure 2(a-b). The pre-event PALSAR image was taken on September 11, 2010 with 41.5° incidence angle, and the post-event image was taken on March 16, 2011 with 43.1° incidence angle. Two images were taken by HH polarization in the descending path, similar with TerraSAR-X images. They were taken by Fine Beam Single Polarization (FBS) Mode, and were processed as the Multi-look amplitude generated intensity images. The resolution of PALSAR images was 6.25 m, which is 1/5 of the TerraSAR-X images. The ALOS sensor had completed its operations on May 12, 2010, thus, this earthquake was the last big event in its observation.

Two pre-processing approaches were applied before the analysis. Firstly, TerraSAR-X images and PALSAR images were transformed to Sigma Naught, which represents the radar reflectivity per unit area in the ground range, to compare them directly. Secondly, Lee filter (Lee, 1980), one of the most common adaptive filters, was used to reduce speckle noises in the original SAR images, which make the radiometric and textural aspects less efficient. To sustain the information included in the intensity images, the window size of Lee filter was set as 3×3 pixels. The portion of images covering about 260 km^2 areas in Higashi-Matsushima city, which is one of the most severely affected areas, was selected as a site for analysis in this study. Color compositions of the processed images were shown in Figure 3, where the pre-event images were loaded as Green and Blue colors while the post-event images as Red color. Since the water surface shows low backscatter, the flooded areas can be seen easily in Cyan (Green plus Blue) color, due to the reduction of backscatters after tsunami. Since X-band is more sensitive to fine undulation than L-band is, the difference between water surface and others was clearer in the TerraSAR-X images than in the PALSAR images. Except for the damage caused by the earthquake/tsunami, Figure 3 also shows Cyan-colored areas at the upstream of Naruse River due to agricultural works (watering to rice paddy fields).

A high resolution DEM was also employed to investigate the occurrence condition of flooded areas obtained from GEO Grid by ASTER AVNIR images. While the Shuttle Radar Topography Mission (SRTM) by NASA is the most common DEM currently, its resolution is about 90m, much worse comparing with the SAR images used here. Hence this study used the ASTER DEM with 15m resolution, made from the pair of AVNIR panchromatic images.

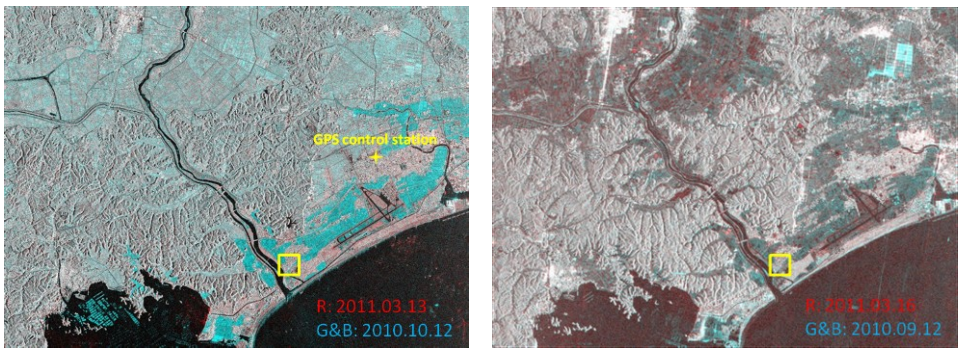

(a) (b)

Figure 3 Color composite of the pre- and post-event TerraSAR-X images (a) and PALSAR images (b) after preprocessing.

The average value of two DEMs made from the images taken on May 5 and September 10, 2010, was used as the pre-event DEM to improve the accuracy, shown in Figure 2(c).

3. FLOODED AREA EXTRACTION

Since the distinction in backscatter between water and other surfaces is very significant, taking the difference between the pre- and post-event SAR images is considered to be the simplest and most efficient method to extract flooded areas.

3.1 TerraSAR-X images

Firstly, the subtraction between the pre- and post-event images was carried on TerraSAR-X images directly. One part of the result is shown in Figure 4(a). The backscatter of flooded areas reduced after the earthquake, shown as a negative change (minus value) in the result. A pre-event optical image quoted from Google Earth and a post-event aerial photograph taken by GSI on March 12, 2011, were used to verify the result, shown in Figure 4(e-f). Comparing the optical images and the difference image, most flooded areas were shown as minus values in the result. However, many negative and positive changes existed surrounding buildings which were not always caused by tsunami. Some of these changes might be caused by crustal movement in this earthquake (Liu and Yamazaki, 2011), and would be extracted as errors in flooded area detection. Note that about 4 m horizontal crustal movement was recorded by GPS measurement (GSI, 2011), and it was detected from the TerraSAR-X intensity images.

Thus, an average difference method was applied in this study. A small window was selected from the pre- and post-event images, respectively, for the same location. The difference between the two average values of backscatter in the windows was calculated as the difference at the center pixel of the window. By this method, the difference would be smoothed, and the errors caused by crustal movement would be reduced. The window size was set as 3×3, 9×9, 15×15 pixels. As the window size became bigger, the result of difference became smoother. The parts of the results are shown in Figure 4(b-d). When the window size was set as 15×15 pixels, the changes cause by the movement of buildings were almost obliterated. Also the shapes of flooded areas were remained well comparing with the optical images. Hence, 15×15 pixels was determined as the most efficient window size to extract flooded areas. The histogram of this difference result is shown in Figure 4(g).

According to the histogram, the small peak in minus values can be inferred as flooded areas. Three different threshold values between this peak and the peak of non-changes were defined to extract flooded areas. When the threshold value was set as -6.4 dB, many other negative changes were extracted as flooded areas, such as the change due to agriculture works and changes of forestry in the mountain. When the threshold value was set as -8.6 dB, several boundaries of flooded areas could not be extracted. Comparing with the optical images, when the threshold value was set as -7.4 dB, the best result was obtained with well shapes and less errors. Hence, the areas with the difference between the pre- and post-event TerraSAR-X images less than -7.4 dB were extracted as the flooded areas.

Although the errors were reduced by using the average difference value, there were still many noises in the results due to the changes in buildings or vehicles (swept away by tsunami). Which were extracted as changes by "sensitive" X-band. Therefore, the extracted objects less than 350 pixels (about 500 m^2) were removed from the result to eliminate these noises. On the other hand, the holes completely surrounded by the extracted objects were filled. Then a sea mask was applied to remove the changes due to aquaculture rafts on the sea. Finally, the extracted flooded areas became approximately 11.5km^2, as shown in Figure 6(a) by the blue color.

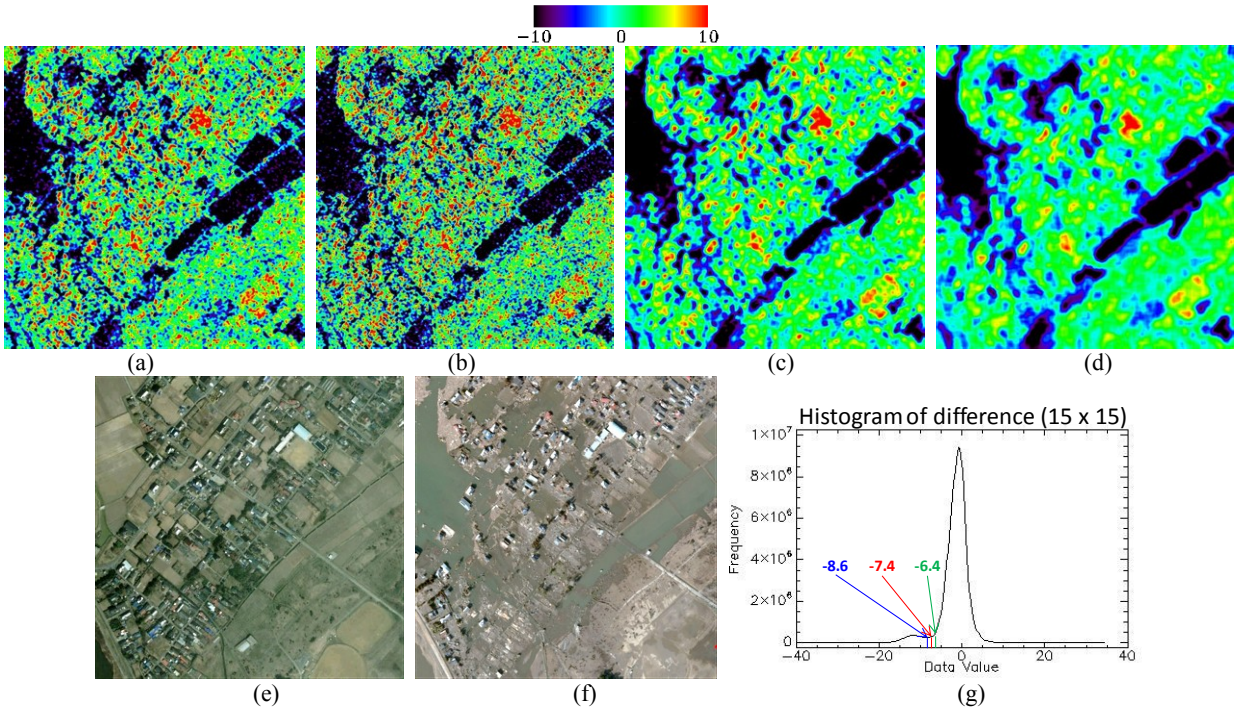

Figure 4 Parts of difference from the pre- and the post-event TerraSAR-X images by different window sizes: (a) non-window, (b) 3×3 pixels, (c) 9×9 pixels, (d) 15×15 pixels; the pre-event optical image quoted from Google Earth (e) and the post-event aerial photograph taken on March 12, 2011 by GSI (f); the histogram of difference calculated by 15×15 pixels window (g).

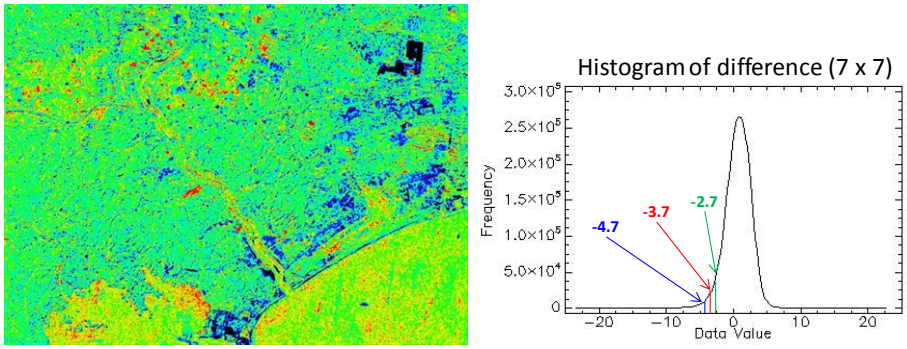

Figure 5 The difference image calculated by 7×7 pixels window from the pre-and the post-event PALSAR images (a) and its histogram (c).

3.2 PALSAR images

The difference between the pre- and post-event PALSAR image was also calculated by the same method to extract flooded areas. Since the incident angle of the pre-event image was 41.5° while the post-event image was 43.1°, the difference exist between the two images even though there was no change, by which the direct subtraction may not provide a good result. The average difference with a smoothing window was carried out with the sizes of 3×3, 5×5, 7×7 and 9×9 pixels. Since the resolution of PALSAR image was 6.25m, which is larger than the crustal movement in this area, the difference of non-changed building in the image was mainly induced by the different incident angle. According to the resolution, which was 1/5 of TerraSAR-X image, the relatively small window sizes were attempted. When the window size was 3×3 or 5×5 pixels, the difference of buildings due to the incident angle could not be removed from the result. When the window size was 9×9 pixels, several small flooded areas could not be distinguished. Hence, the best window size was set as 7×7 pixels, whose results are shown in Figure 5(a), with its histogram in Figure 5(b).

Different from the TerraSAR-X images, it was difficult to select a threshold value to extract flooded areas from the histogram of the PALSAR images. Then the mean value μ and standard deviation σ were used to extract flooded areas by ranging the threshold value as μ-σ, μ-1.5σ and μ-2σ, where μ and σ were obtained as -0.73 dB and 1.97 dB, respectively. When the threshold value was -2.70 dB corresponding to μ-σ, the most of the areas colored by cyan in Figure 3(b) were extracted as flooded areas, which includes many errors caused by the different incident angles.

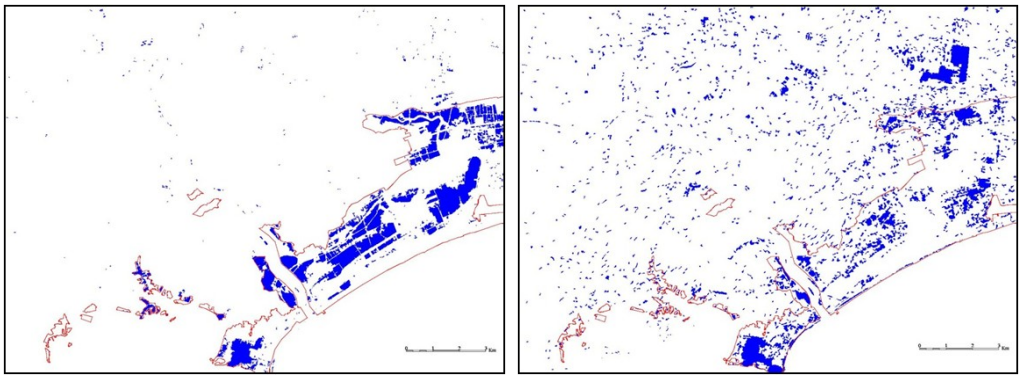

(a) (b)

Figure 6 Results of extracted flooded areas from TerraSAR-X images (a) and PALSAR images (b); the result of visual detection by PASCO was shown in red lines.

When the threshold value was set as -3.69 dB (μ-1.5σ) or -4.67 dB (μ-2σ), many boundaries of flood areas could not be extracted. Hence, the threshold value of -2.7 dB was selected to extract flooded areas from the difference of backscatter between the pre- and post-event images. The extracted flooded areas became approximately 14.5km^2, as shown in Figure 6(b) by the blue color. As a result, many errors were caused by the changes of agriculture fields existed and due to the foreshortening of mountains' peaks by different incident angles.

4. VERIFICATION AND INVESTIGATION

4.1 Verification of extracted results

A shape file of the estimated inundated areas made by PASCO was used to verify the accuracy of the extracted flooded areas (PASCO, 2011). The inundated areas by PASCO were obtained by visual interpretation of several images before and after the earthquake taken by different optical and SAR sensors including TerraSAR-X, ALOS/PRISM and AVNIR-2, Worldview-1, 2 and RapidEye. The inundated areas were approximately 39 km^2 in this study area continuously distributing along the coastline, whereas the extracted flooded areas from the SAR images were narrower and discontinuous. These differences were caused by two reasons. First, the difference extraction from SAR images could only extract the ground areas which became water bodies after tsunami. Thus, the flooded urban areas with buildings left standing could not be extracted by this method. Secondly, the run-up boundaries were those tsunami reached, which were estimated from the images taken some times after tsunami and from debris distribution, while our flooded areas were those covered by water when the post-event images were obtained. Obviously, the flooded area became narrower and narrower as time went. However, the run-up boundaries were used as the reference to verify the accuracy of extraction in this study. The accuracy of the results was summarized in Table 1.

The overall accuracy from the TerraSAR-X images is 89%, while from the PALSAR images is 85%. 96% of the extracted flooded areas were correct in case of the TerraSAR-X images while 49% in case of the PALSAR images. The errors in PALSAR were mainly caused by the different incident angles of the pre- and post-event images. Although the smooth window removed the difference of buildings, the difference of mountain peaks with high elevation could not be smoothed. Another reason of errors for L-band is that paddy fields show similar low backscatter as flooded areas. Since X-band is sensitive to small undulation, flooded areas could be distinguished from paddy fields by their lower backscatter in the TerraSAR-X images. Hence, X-band is considered to be more suitable than L-band in extraction of flooded areas.

4.2 Relationship between flooded areas and DEM

The pre-event ASTER DEM was compared with the correctly extracted flooded areas from the TerraSAR-X images. The histogram of DEM is shown in Figure 7(a), separating flooded areas and non-flooded areas. Since more than half of the target areas are located on a plain with urban and farm land use, the elevation is concentrated around 40 to 80 m (90%). The elevation of extracted flooded areas distributed a narrow range, around 40 to 45 m. The slop angle was calculated from the DEM data, shown in Figure 7(b). There were several high mountains in this area and the slope angles distributed from 0 to 52 degrees; the angle from 0 to 10 degrees shared the most part. The slope of flooded areas is lower than 8 degrees. Hence, the elevation less than 50 m and slope less than 10 degrees can be considered as additional parameters to improve the accuracy of flooded area extraction for this site.

Table 1 Accuracy of the extracted result from TerraSAR-X images (a) and PALSAR images (b)

(a)

		Inundation map from PASCO			
		Non-flooded area	Flooded area	Total	User accuracy
Result from PALSAR images	Non-flooded area	82.24%	12.30%	94.54%	86.99%
	Flooded area	2.76%	2.70%	5.46%	49.48%
	Total	85.00%	15.00%	100.00%	
	Producer accuracy	96.76%	18.00%		84.94%

(b)

		Inundation map from PASCO			
		Non-flooded area	Flooded area	Total	User accuracy
Result from TerraSAR-X images	Non-flooded area	84.82%	10.73%	95.55%	88.77%
	Flooded area	0.18%	4.27%	4.45%	95.92%
	Total	85.00%	15.00%	100.00%	
	Producer accuracy	99.79%	28.47%		89.09%

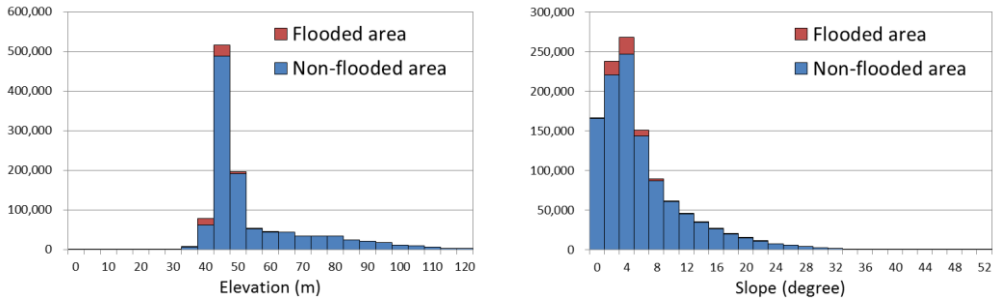

(a) (b)

Figure 7 Histogram of DEM (a) and slope (b), showing the breakdown of non-damaged and flooded areas.

5. CONCLUSIONS

In this study, a simple difference method was applied on the pre- and post-event TerraSAR-X and PALSAR intensity images to extract flooded areas after the 2011 Tohoku earthquake/tsunami. The most suitable parameters in the smoothing window size and its threshold value were discussed to obtain the highest accuracy. From the both pairs of SAR images, the flooded areas were extracted successfully. However, the result from the TerraSAR-X images shows higher accuracy. Comparing the correctly extracted flooded areas with the 15 m resolution ASTER DEM, the flooded areas were concentrated at the low elevation and small slope-angle locations. These relationships may improve the accuracy of flooded area extraction in future.

ACKNOWLEDGEMENTS

The TerraSAR-X images used in this study were provided to the present authors from Pasco Corporation, Tokyo, Japan, as one of the granted projects of the SAR data application research committee. The PALSAR images were provided from Remote Sensing Technology Center of Japan (RESTEC) and the ASTER DEM was provided from GEO Grid, National Institute of Advanced Industrial Science and Technology (AIST), Tsukuba, Japan.

REFERENCES

Ahton, P., Euro, M., Hallikainen, M., Solbø, S., Johansen, B., and Solheim, I., 2004. SAR and optical based algorithms for estimation of water bodies. Technical report, FloodMan Project.

Dellepiane, S., Bo, G., Monni, S., and Buck, C., 2000. SAR images and interferometric coherence for flood monitoring. In: Proceeding of Geoscience and Remote Sensing Symposium, Vol.XI, pp. 2608-2610.

Geudtner, D., Winter, R., Vachon, P., 1996. Flood monitoring using ESR-1 SAR interfermometry coherence maps. In: Proceeding of Geoscience and Remote Sensing Symposium, Vol.II, pp. 966-968.

GSI, 2011. http://www.gsi.go.jp/BOUSAI/h23_tohoku.html.

Heremans, R., Willekens, A., Borghys, D., Verbeeck, B., Valckenborg, J., Acheroy, M., and Perneel., C., 2003. Automatic detection of flooded areas on ENVISAT/ASAR images using an object-oriented classification technique and an active contour algorithm. In: Proceeding IEEE Conference on Recent Advances in Space Thechnologies, pp: 289-294.

Horritt, M.S., 1999. A statistical active contour model for SAR image segementation. Image and Vision Computing, 17, pp: 213-224.

Lee, J. S., 1980. Digital image enhancement and noise filtering by use of local statistics. Transactions on Pattern Analysis and Machine Intelligence, PAMI-2 (2), Institute of Electrical and Electronics Engineers, pp. 165–168.

Liu, W., and Yamazaki, F., 2011. Estimation of crustal movements due to the 2011 Tohoku, Japan Earthquake from TerraSAR-X intensity images. Ninth International Workshop on Remote Sensing for Disaster Response, 10p.

Matgen, P., Schumann, G., Henry, J.-B., Hoffmann, L., and Pfister, L., 2007. Integration of SAR-derived inundation areas, high precision topographic data and a river flow model toward real-time flood management. Journal of Applied Earth Observation and Geoinformation, 9, pp: 247-263.

PASCO, 2011. http://www.pasco.co.jp/disaster_info/110311/.